 Human Molecular Genetics, 2002, Vol. 11, No. 3 217–227

Assembly and iron-binding properties of human frataxin, the protein deficient in Friedreich ataxia

Patrizia Cavadini, Heather A. O'Neill, Oldrich Benada[1] and Grazia Isaya*

Departments of Pediatric and Adolescent Medicine, and Biochemistry and Molecular Biology, Mayo Clinic and Foundation, Rochester, MN 55905, USA and [1]Institute of Microbiology, Academy of Sciences of the Czech Republic, Prague, Czech Republic

Received September 4, 2001; Revised and Accepted November 28, 2001

Friedreich ataxia (FRDA) is an autosomal recessive degenerative disease caused by a deficiency of frataxin, a conserved mitochondrial protein of unknown function. Mitochondrial iron accumulation, loss of iron-sulfur cluster-containing enzymes and increased oxidative damage occur in yeast and mouse frataxin-depleted mutants as well as tissues and cell lines from FRDA patients, suggesting that frataxin may be involved in export of iron from the mitochondria, synthesis of iron-sulfur clusters and/or protection from oxidative damage. We have previously shown that yeast frataxin has structural and functional features of an iron storage protein. In this study we have investigated the function of human frataxin in *Escherichia coli* and *Saccharomyces cerevisiae*. When expressed in *E.coli*, the mature form of human frataxin assembles into a stable homopolymer that can bind approximately 10 atoms of iron per molecule of frataxin. The iron-loaded homopolymer can be detected on non-denaturing gels by either protein or iron staining demonstrating a stable association between frataxin and iron. As analyzed by gel filtration and electron microscopy, the homopolymer consists of globular particles of ~1 MDa and ordered rod-shaped polymers of these particles that accumulate small electron-dense cores. When the human frataxin precursor is expressed in *S.cerevisiae*, the mitochondrially generated mature form is separated by gel filtration into monomer and a high molecular weight pool of >600 kDa. A high molecular weight pool of frataxin is also present in mouse heart indicating that frataxin can assemble under native conditions. In radiolabeled yeast cells, human frataxin is recovered by immunoprecipitation with approximately five atoms of ^{55}Fe bound per molecule. These findings suggest that FRDA results from decreased mitochondrial iron storage due to frataxin deficiency which may impair iron metabolism, promote oxidative damage and lead to progressive iron accumulation.

INTRODUCTION

Friedreich ataxia (FRDA) is an autosomal recessive degenerative disease clinically characterized by progressive ataxia of all four limbs, cerebellar dysarthria, absent reflexes in the lower limbs, sensory loss, and pyramidal signs (1). Cardiomyopathy is found in most patients and represents the most frequent cause of premature death (1). The FRDA locus encodes a precursor polypeptide that is imported by the mitochondria and processed to a 155 amino acid protein designated frataxin (2–4). Most patients are homozygous for a large GAA repeat expansion in the first intron of the FRDA gene which impairs transcription, ultimately causing a severe reduction in the levels of frataxin (reviewed in 5). How frataxin deficiency leads to neuro- and cardio-degeneration is still unknown but potential pathogenic mechanisms are emerging from studies in yeast and mouse, which are made possible by the fact that frataxin is conserved in eukaryotes (6). Yeast frataxin knock-out mutants typically show accumulation of iron in mitochondria and loss of respiration (3,7–9). Mutant mice in which the frataxin gene is selectively inactivated in neuronal and cardiac tissues develop neuronal sensory defect and cardiomyopathy at the same time as mitochondrial iron-sulfur enzyme deficiencies, and show at a later stage mitochondrial iron accumulation (10). It has been proposed that these phenotypes may result from impaired mitochondrial iron efflux (11,12), defective biosynthesis of iron-sulfur clusters (13–15) or disabled antioxidant defenses (16), with each of these conditions in turn leading to mitochondrial iron overload and oxidative damage. The observation that the mitochondrial inner membrane potential and ATP synthesis are increased in cultured cells overexpressing human frataxin has suggested another pathogenic mechanism in which frataxin deficiency leads to loss of oxidative phosphorylation while mitochondrial iron accumulation is a secondary effect due to ATP depletion (17). Support for each of these models is provided by evidence of abnormal cellular iron homeostasis (18–22), increased oxidative damage (23–25) and respiratory deficits (19,26,27) in tissues and cell lines derived from FRDA patients.

*To whom correspondence should be addressed. Tel: +1 507 266 0110; Fax: +1 507 266 9315; Email: isaya@mayo.edu

The authors wish it to be known that, in their opinion, the first two authors should be regarded as joint First Authors

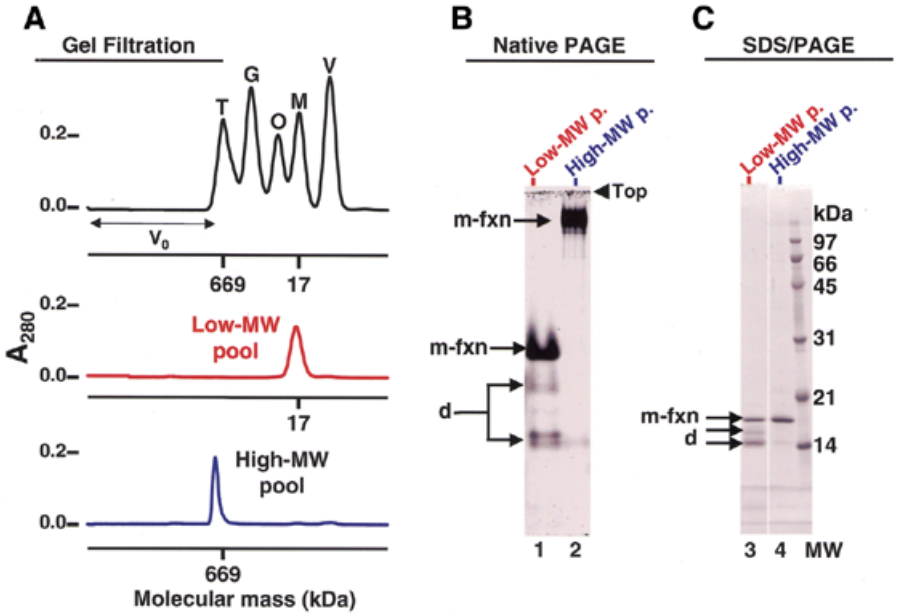

Figure 1. Isolation of low- and high-MW pools of m-fxn from *E.coli*. (**A**) Two different pools of overexpressed m-fxn were isolated from the bacterial lysate by ion-exchange chromatography, and each pool was analyzed by gel filtration. The top chromatogram shows the elution profile of MW standards: V, vitamin B_{12} (1.4 kDa); M, myoglobin (17 kDa; 81.8 ml elution volume); O, ovalbumin (44 kDa); G, gammaglobulin (158 kDa); T, thyroglobulin (669 kDa; 45.1 ml elution volume). A_{280}, absorbance at 280 nm; V_o, void volume (41.2 ml). The elution profiles of the low- and high-MW pool of m-fxn are also shown. Elution volumes were 80.6 ml for the low-MW pool and 41.6 ml for the high-MW pool. (**B**) Native PAGE and (**C**) SDS–PAGE of the low- and high-MW pools isolated by gel filtration. Samples from each pool were analyzed by 7% native PAGE (5 µg total protein per lane; lanes 1–2; arrowhead shows the top of the separating gel), or 12% SDS–PAGE (1 µg total protein per lane; lanes 3–4; MW, molecular weight markers), and Sypro Orange staining. d, degradation products of m-fxn.

We have proposed that the involvement of frataxin in such diverse functions as iron efflux, iron-sulfur cluster biogenesis, stimulation of oxidative phosphorylation and protection from oxidative damage could be rationalized if this protein were able to keep iron in soluble and non-toxic form (5). This hypothesis is supported by our previous observation that yeast frataxin assembles with itself and binds iron in stable form (28). In this study, we have expressed human frataxin in *Escherichia coli* and *Saccharomyces cerevisiae* and have analyzed its ability to assemble and bind iron. Consistent with a role in iron management, we show that human frataxin has structural and functional features of an authentic iron storage protein.

RESULTS

Isolation of a high molecular weight form of human frataxin from *E.coli*

Human frataxin is normally synthesized as a precursor polypeptide with a mitochondrial matrix targeting signal of 55 amino acids that is cleaved by mitochondrial processing peptidase to yield the mature form (m-fxn) (4). When overexpressed in *E.coli*, m-fxn (residues 56–210 plus an initiator methionine residue at the N-terminus) was soluble and exhibited the expected molecular weight (MW) of ~17 000 on SDS–PAGE. This protein was purified from the bacterial lysate in three chromatographic steps. Ion-exchange chromatography yielded two different m-fxn fractions that eluted at low and high salt concentrations, respectively (data not shown). As analyzed by Superdex 200 gel filtration, the low-salt fraction had an apparent MW of ~17 000 while the high-salt fraction eluted at the size exclusion limit of the column, consistent with a MW of >600 000 (Fig. 1A, low- and high-MW pool). Both pools were isolated from the soluble fraction of the bacterial lysate, not from insoluble inclusion bodies. In particular, the high-MW pool remained soluble after centrifugation of the total lysate at 25 000 *g* for 20 min and throughout the isolation procedure, and continued to be soluble in purified form at a protein concentration of at least 2 mg/ml.

Non-denaturing PAGE of the low- and high-MW pools isolated by gel filtration revealed two major protein bands of different electrophoretic mobility (Fig. 1B). However, SDS–PAGE showed that both pools contained the same species, including an ~17 kDa protein and smaller products ≥14 kDa (Fig. 1C). Electrospray ionization mass spectrometry (ESI-MS) confirmed the presence in the low-MW pool of a predominant species of 17 252 Da corresponding within experimental error to full-length m-fxn without the N-terminal methionine, that was cleaved during expression in *E.coli* (29). ESI-MS also detected a second species of 14 663 Da corresponding to residues 78–210 of m-fxn. Similarly, Pastore and co-workers (30) reported previously that bacterially expressed human frataxin was naturally and quantitatively degraded during purification into a 14 kDa product. This species is ~20 residues shorter than the mature form and very likely corresponds to a major degradation product of human frataxin that was originally observed during import of the human frataxin precursor into isolated rat liver mitochondria (4).

ESI-MS of the high-MW pool could not detect the macromolecular species observed by gel filtration and non-denaturing PAGE, as expected (31), but did detect low levels of full-length

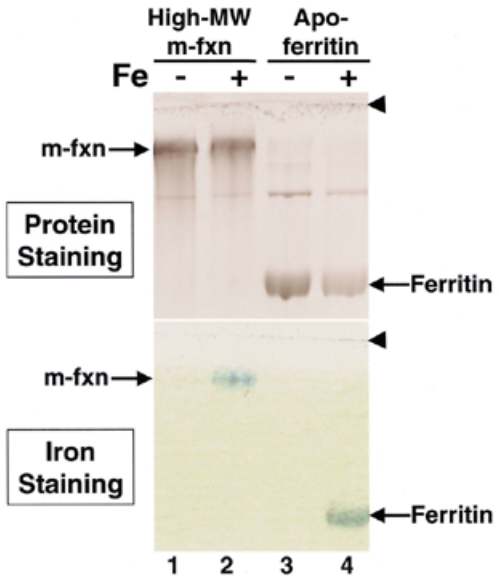

Figure 2. Iron loading of high-MW m-fxn. Purified high-MW m-fxn (50 µg per lane; lanes 1–2) and horse spleen apoferritin (12.5 µg per lane; lanes 3–4) were analyzed in duplicate on 7% native PAGE. Prior to PAGE, samples in lanes 2 and 4 were iron loaded as described in Materials and Methods. One-half of the gel was stained for proteins with Sypro Orange and the other half for ferric iron with Prussian Blue. Arrowheads show the top of the separating gel.

m-fxn and the 14 kDa product (data not shown). In purified form, low-MW m-fxn was spontaneously and progressively degraded into the 14 kDa product. In contrast, high-MW m-fxn was stable for several days at room temperature or 4°C. These results indicate that stable polymers of full-length m-fxn are formed during overexpression in *E.coli*.

Iron loading of high-MW m-fxn

As purified from bacterial cells, high-MW m-fxn contained fewer than one atom of iron per molecule of m-fxn, as determined by inductively coupled plasma emission spectroscopy (ICP) on four different protein isolations. After incubation with ferrous iron, however, iron levels increased to 7–10 Fe/molecule of m-fxn (range of values from five independent experiments). A similar behavior has been described for overexpressed bacterial ferritins and recombinant human ferritin homopolymers, that contain low iron levels as isolated from bacterial cells but can subsequently be loaded with iron *in vitro* (32–34). Similar to ferritin, iron-loaded m-fxn was detected as one discrete band by either protein or iron staining on 7% native PAGE (Fig. 2). This result demonstrates that protein and iron are associated in one stable and soluble macromolecular complex. The electrophoretic mobility of iron-loaded m-fxn was not changed compared to untreated m-fxn, as was the case for ferritin compared to apoferritin, indicating that iron is stored within these proteins and that iron loading does not result in protein aggregation.

We showed previously that the yeast frataxin monomer does not have any tendency to assemble during overexpression in *E.coli* but assembles *in vitro* in the presence of high Fe^{2+}/protein ratios (28). In contrast, the human frataxin monomer assembled spontaneously in *E.coli* (high-MW pool) but only minimally (<10% of the low-MW pool) when treated with increasing iron concentrations *in vitro* (data not shown). The concentration of 'free' iron has been estimated to be in the order of 10^{-5} M in *E.coli* (35), which is close to the 'free' iron concentration found in mammalian mitochondria (4.8–9.2 µM) (36). Thus, we can assume that assembly of human frataxin in *E.coli* occurs in the presence of physiologic concentrations of iron. The inability of purified human frataxin monomer (i.e. the low-MW pool) to undergo self-assembly *in vitro* suggests that, unlike yeast frataxin, human frataxin requires additional assembly factors that remain to be identified. The low-MW pool does not assemble in *E.coli* either, however, and may therefore represent protein incompetent for assembly. Similarly, only ~70% of the total yeast frataxin monomer obtained from *E.coli* is able to undergo self-assembly (28).

Human frataxin is an iron storage protein

Electron microscopy (EM) of high-MW m-fxn stained with uranyl acetate shows elongated rod-shaped structures of variable lengths but uniform diameter of ~16 nm (Fig. 3A). Isolated and apparently globular particles are less frequently detected (Fig. 3A and B). The edges of the rods are indented at regular intervals, giving the appearance of individual particles stacked on top of one another forming dimers, trimers and longer polymers (Fig. 3B). We have consistently observed these structures in four different protein isolations, independent of iron loading. Elongated structures are also present in unstained samples of iron-loaded high-MW m-fxn (Fig. 3A and C). These structures consist of chains of small electron-dense iron cores; isolated cores are less frequently detected (Fig. 3A and C). Multiple electron-dense granules were previously observed in electron micrographs of yeast frataxin multimer (28). A smaller number of iron granules appear to be present in human frataxin particles, which is explained by a ~5-fold difference in iron-binding capacity between yeast (~50 Fe/molecule) (28) and human frataxin (~10 Fe/molecule). Size-wise, the structures detected by negative staining correspond to those detected in unstained samples (Fig. 3D). Dimers, trimers and longer polymers of apoferritin particles are occasionally seen in negatively stained apoferritin samples (Fig. 3A and B) and more frequently in ferritin samples (Fig. 3A and C). The iron cores of ferritin are larger than those of m-fxn, consistent with the much higher iron-binding capacity of the former protein (up to 187 Fe/molecule) (37). These results confirm that m-fxn can assemble with itself and store iron in mineral form, similar to ferritin. In agreement with these data, other investigators have previously noted conserved structural features that may enable human frataxin to assemble with itself and form a negatively charged cavity similar to the anionic surface involved in the iron storage mechanism of ferritin (30,38).

A tendency to form stable polymers has been previously reported for apoferritin and ferritin particles (39–41), and can be observed in Figure 3B and especially Figure 3C. A very similar phenomenon has also been described for the spinach chloroplast protein, cpn21 (42), and the oat chloroplast protein, β-glucosidase (43). Electron micrographs of bacterially expressed cpn21 or β-glucosidase show circular molecules and fibrillar polymers of different lengths that consist of individual circular molecules stacked on top of one another (42,43), remarkably similar to the rod-shaped structures formed by m-fxn. Fibrillar polymers of oat β-glucosidase exist in the chloroplast

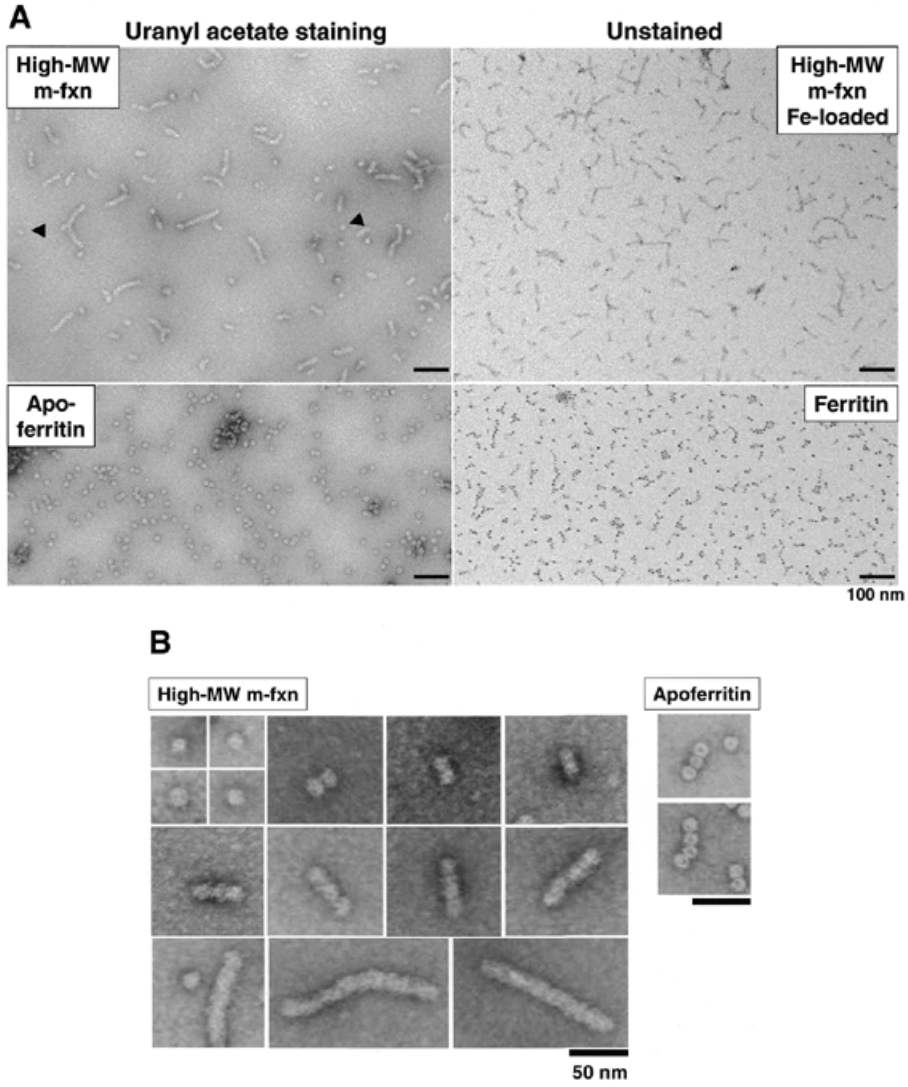

Figure 3. (Above and opposite) Electron microscopy of high-MW m-fxn. (**A**–**D**) Samples (~0.1 mg/ml) of high-MW m-fxn or apoferritin were stained with 2% uranyl acetate, whereas iron-loaded high-MW m-fxn or ferritin were absorbed on a grid and analyzed without further manipulations. The accelerating voltage was 80 kV and the initial magnification was 64 000×. Arrowheads indicate isolated particles or iron cores.

stroma and are believed to be important for β-glucosidase function (43). On the other hand, ferritin polymers have been attributed to partial denaturation of the protein shell that exposes hydrophobic parts to the aqueous environment promoting hydrophobic interactions and thus oligomerization (41). The significance of human frataxin polymers is not known at this time. When yeast frataxin particles are assembled *in vitro* from purified monomer they show little tendency to polymerize (28 and unpublished data). This suggests that polymerization of human frataxin particles may result from overproduction in *E.coli* and mechanical stress during purification from bacterial cells. It is important to note, however, that the rod-shaped polymers are soluble, stable and ordered structures that retain the ability to bind iron (Fig. 3A–D), and are therefore unlikely to be the product of random protein aggregation. Thus, although the functional significance of the rod-shaped polymers remains to be elucidated, we can conclude that they reflect a natural tendency of human frataxin to assemble with itself and form higher-order structures.

The high-MW pool consists of m-fxn molecules ranging from ~1 to several MDa

In order to estimate the molecular mass of high-MW m-fxn, this pool was fractionated on a Sephacryl 300 column (fractionation range 1×10^4–1.5×10^6; exclusion limit up to 400 nm) calibrated with different multimeric proteins and polymers of known molecular mass (Fig. 4A). Most protein eluted in one bell-shaped peak that raised near the elution volume of Blue Dextran (2 MDa; fraction 38), and dropped near the elution volume of the apoferritin polymers (>1.3 MDa; fraction 39), followed by a small tail (fraction 40) near the elution volume of the yeast frataxin multimer (~1.1 MDa; fraction 41) (Fig. 4A). Fractions were analyzed by 5% native PAGE and western blotting with anti-human frataxin antibodies. No protein was

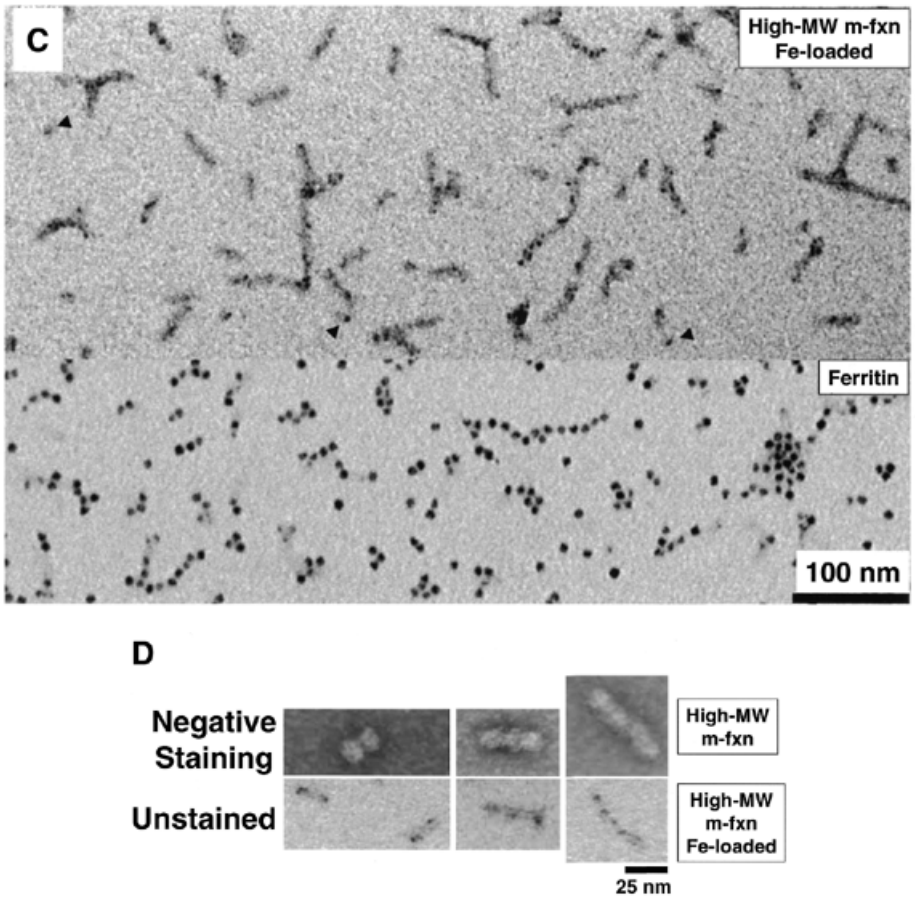

detected in the void volume (fraction 36) by either Sypro Orange staining (not shown) or western blotting (Fig. 4B). Two diffuse bands were detected in fractions 38–42: a slower band (denoted β) whose elution profile corresponded to the main peak, and a faster band (denoted α) whose elution profile corresponded to the peak's tail (Fig. 4B). The diffuse appearance of these bands suggested that each might represent a ladder of species that could not be clearly resolved on 5% native PAGE. This was confirmed by EM analysis. Fraction 38, which contained mostly β and only traces of α (Fig. 4B), showed a predominance of rod-shaped polymers and a few isolated globular particles (Fig. 4C). Fraction 40, which contained higher levels of α (Fig. 4B), showed a greater proportion of individual particles as well as rod-shaped oligomers (Fig. 4C). These results are consistent with a distribution of m-fxn macromolecules ranging from globular particles with a molecular mass close to that of the yeast frataxin multimer (~1.1 MDa) to long polymers of these particles with a molecular mass in excess of several MDa. A distribution of species is similarly observed for apoferritin, except that the apoferritin particle (MW 440 000) is well within the fractionation range of Sephacryl 300 and can be clearly separated from its dimer and longer polymers (Fig. 4A). The m-fxn particle (~1.1 MDa) is at the limit of the fractionation range of Sephacryl 300 which only allows partial separation between long polymers (β band) and short oligomers/particles (α band).

Assembly of m-fxn in *S.cerevisiae* and mouse heart

We showed previously that human frataxin rescues the respiratory-deficient phenotype with mitochondrial iron accumulation characteristic of the yeast frataxin knock-out model (44). High-MW frataxin should therefore be detected in the complemented *yfh1*Δ[FRDA] strain if protein assembly and iron binding are relevant to the protein's ability to maintain normal mitochondrial iron levels. Total cell extracts were prepared from this strain under non-denaturing conditions, and were size-fractionated through a Superdex 200 gel filtration column (fractionation range 10–600 kDa) calibrated with different proteins of known molecular mass (Fig. 5A). Fractions that eluted between the void volume and a molecular mass ≥5 kDa were analyzed by SDS–PAGE and western blotting, sequentially probing the same membrane with polyclonal anti-human frataxin antibodies and a monoclonal anti-yeast phosphoglycerate kinase (Pgk1p) antibody. Mature frataxin (i.e. protein produced by cleavage of frataxin precursor by mitochondrial processing peptidase in the mitochondrial matrix; m-fxn) (4) and its degradation products (d) were detected in all fractions (Fig. 5A). Degradation of m-fxn was more pronounced for low-MW m-fxn (fractions 11–12) compared to high-MW m-fxn (fractions 1–2), as already observed for the low- and high-MW pools isolated from *E.coli* (compare Figs 5A and 1C). The levels of m-fxn and its degradation products were measured by densitometry and the sum was considered the total amount

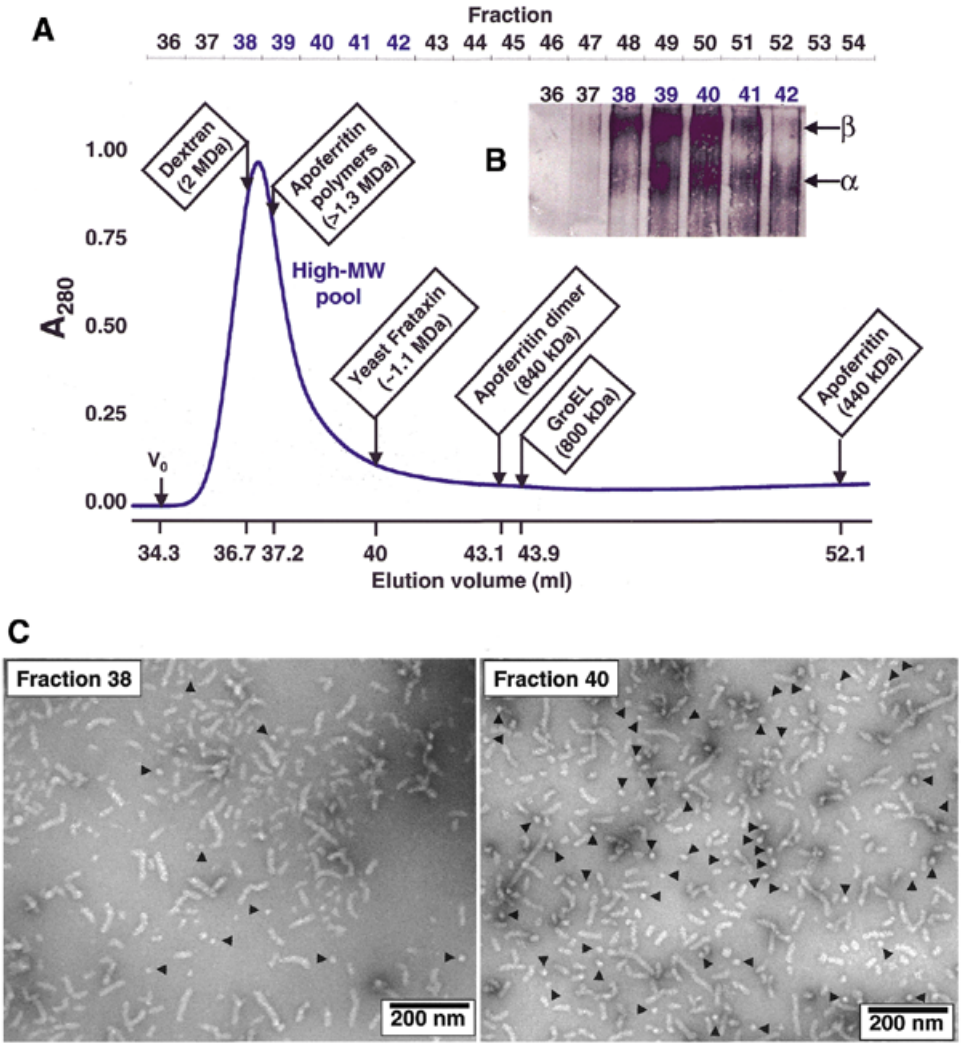

Figure 4. Size-fractionation of high-MW m-fxn. (**A**) High-MW m-fxn was isolated from the bacterial lysate by ion-exchange chromatography, and further analyzed by gel filtration on a column packed with Sephacryl 300. The chromatogram shows the elution volumes of different multimeric proteins and polymers. A_{280}, absorbance at 280 nm; V_o, void volume. The elution profiles of high-MW m-fxn is shown in blue. The elution volume of the m-fxn peak was 36.8 ml. (**B**) Ten microliters from each of the fractions corresponding to the m-fxn peak were analyzed by 5% native PAGE and western blotting with anti-human frataxin antibodies. Only the relevant portion of the blot is shown. (**C**) Aliquots (~0.1 mg total protein/ml) of fractions 38 and 40 were stained with 2% uranyl acetate and analyzed by EM as described in the legend of Figure 3. Arrowheads indicate isolated particles.

of mature frataxin eluted in each fraction. By both visual inspection of western blots and densitometric measurements it is apparent that mature frataxin eluted in two main peaks, a high-MW peak with molecular mass >600 kDa (fractions 1–2) and a low-MW peak with the expected molecular mass of 17 kDa (fractions 11–12). In contrast, the internal control, Pgk1p, eluted in a single peak with the expected molecular mass of ~45 kDa (Fig. 5A, fractions 8–10).

We also tested whether a high-MW pool of m-fxn could be detected under physiological conditions. A total extract was prepared from mouse heart and was analyzed by gel filtration and western blotting as described above. Short chain acyl-CoA dehydrogenase (SCAD), a 42 kDa mitochondrial matrix protein that assembles into a homotetramer of ~170 kDa (45), was used as the internal control. By both visual inspection of western blots (Fig. 5B) and densitometric measurements (Fig. 5C), the elution profile of the endogenous mouse frataxin was remarkably similar to that of the human protein expressed in yeast. Degradation of mature frataxin was more pronounced in the heart extract compared to the yeast extract, but in both cases the high-MW pool was more stable compared to the monomer pool (Fig. 5A and B). These findings were independently confirmed in several yeast cell extracts and two mouse heart extracts.

Superdex 200 chromatography was chosen for these experiments because it can clearly separate low-MW from high-MW m-fxn in a relatively short period of time compatible with the rate of m-fxn degradation. This particular support, however, cannot separate molecules >600 kDa. In addition, EM analysis of yeast- or mouse-derived high-MW frataxin was not feasible due to low levels of frataxin relative to the total protein present (~0.1 μg m-fxn/mg total protein). We were, therefore, unable

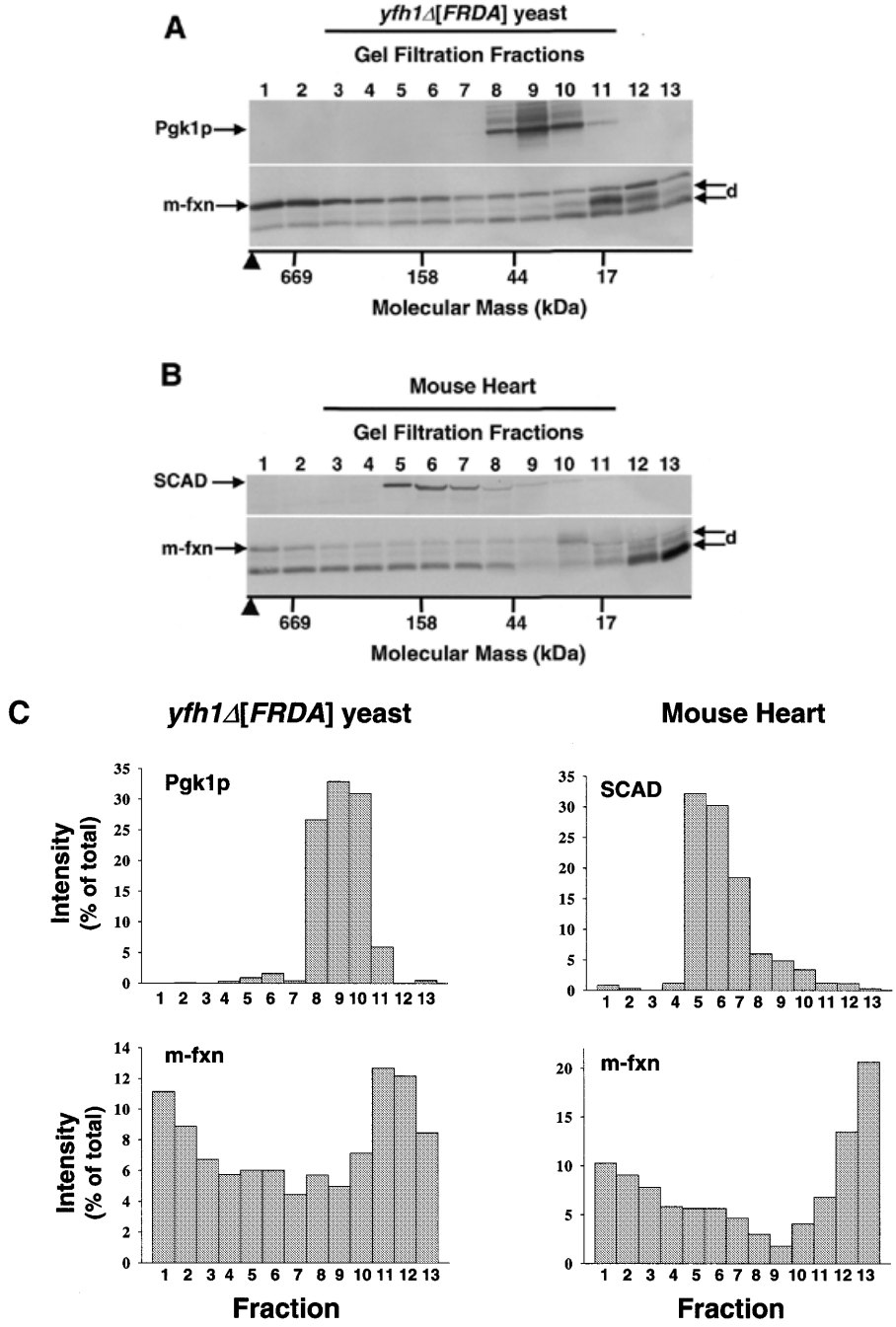

Figure 5. Analysis of m-fxn assembly in yeast cells and mouse heart. (**A**) A total yeast cell extract (~12 mg total protein) was prepared from the *yfh1*Δ[FRDA] strain (44); (**B**) a total tissue extract was prepared from mouse heart (~10 mg total protein) as described in Materials and Methods. Each extract was centrifuged at 100 000 *g* for 30 min and the supernatant was immediately analyzed by Superdex 200 gel filtration. Fractions (0.5 ml each) that eluted between the void volume and molecular mass ≥5 kDa were analyzed by western blotting. The arrowhead indicates the void volume. Molecular masses were deduced from the elution volumes of MW markers as in Figure 1A. The same membrane was probed sequentially with polyclonal anti-human frataxin antibodies and a monoclonal anti-Pgk1p antibody (blot A), or polyclonal anti-SCAD antibodies (blot B). Only the relevant portions of the blots are shown. The 14 kDa product and additional degradation products (d) are detected in all fractions due to degradation of m-fxn during the manipulations that followed fraction collection. The highest levels of degradation are seen in the low-MW pool (fractions 11–12), as observed for bacterially expressed m-fxn (Fig. 1C). (**C**) The intensity of the m-fxn and d bands was measured by densitometry on a STORM 840 with the ImageQuant 5.0 software (Molecular Dynamics). The intensity of the m-fxn plus d bands was considered the total amount of mature frataxin eluted in each fraction, and was expressed as a percentage of the total intensity measured in all fractions.

to define whether the high-MW pools of m-fxn detected in yeast cells and mouse heart consist of isolated particles, polymers or both. Immediately before gel filtration, however, each extract was centrifuged at 100 000 *g* for 30 min as described in Materials and Methods, a procedure expected to eliminate insoluble material. Thus, the main conclusion that can be

Table 1. Binding of ^{55}Fe by m-fxn in the *yfh1*Δ[FRDA] strain

Protein A	Preimmune serum + protein A	Anti-fxn antibodies + protein A
0.74 ± 0.52	0.34 ± 0.18	5.55 ± 2.15
	P = 0.1 versus protein A	P = 0.002 versus protein A

Data represent the percentage of the total c.p.m. measured in each yeast cell extract before any treatment (~13.5×10^6 c.p.m., equal to ~9 nmol ^{55}Fe). The means ±SD determined in six independent experiments are shown.

drawn from these experiments is that both yeast cells expressing human frataxin and mouse heart expressing normal levels of endogenous mouse frataxin contain a soluble high-MW pool of m-fxn. This indicates that frataxin assembly can occur not only during overexpression in *E.coli* but also in eukaryotic cells and under physiologic conditions. It is, therefore, reasonable to conclude that ability to assemble is a natural property of frataxin. The extent to which frataxin assembly occurs in mammalian cells and how this process is regulated are critical questions that remain to be addressed in future studies.

Iron loading of human frataxin in *S.cerevisiae*

To test iron binding by m-fxn *in vivo*, yeast cells were grown in the presence of ^{55}Fe and m-fxn was immunoprecipitated from total cell extracts. In six independent experiments, ~0.5 nmol ^{55}Fe were immunoprecipitated from each extract (corresponding to ~0.5 g cells) by anti m-fxn antibodies plus protein A–Sepharose. This amount was consistently and significantly above background levels of ^{55}Fe recovered by treatment of each extract with protein A–Sepharose alone or a pre-immune serum plus protein A–Sepharose (Table 1). The amount of ^{55}Fe immunoprecipitated from each extract (~0.5 nmol) corresponds to ~50% of the estimated total mitochondrial iron present (~0.9 nmol, estimated as described in Materials and Methods). This proportion is consistent with the presence in mitochondria of a pool of 'non-heme/non-iron-sulfur' iron corresponding to ~30% of the total mitochondrial iron (46) and the fact that *yfh1*Δ[*FRDA*] mitochondria contain twice as much total iron as wild-type mitochondria (44). The concentration of m-fxn was determined by western blotting using purified m-fxn as the internal standard. We measured ~0.1 nmol m-fxn/extract and calculated a molar ^{55}Fe:m-fxn ratio of ~5:1.

DISCUSSION

We have investigated the function of human frataxin, the protein deficient in Friedreich ataxia (2). The mature form of this protein was expressed in *E.coli* and a full-length human frataxin precursor in *S.cerevisiae*. In both experimental systems, the protein has displayed structural and functional features consistent with a role in iron-storage, as observed previously for yeast frataxin (28). Human frataxin was isolated from *E.coli* as a large homopolymer that accumulated at least 10 atoms of iron per subunit *in vitro* and was detected by either protein or iron staining on non-denaturing gels, demonstrating a stable association between frataxin and iron. Accordingly, protein particles and higher order polymers of these particles containing small iron cores were visualized by EM. These findings were confirmed in a *S.cerevisiae* strain carrying a genetically inactivated yeast frataxin gene in which human frataxin was detected as a high-MW species and bound approximately five atoms of ^{55}Fe per subunit in metabolically labeled cells. In this experimental system, the mature protein is physiologically produced via mitochondrial import and processing of the full-length human frataxin precursor and is able to fully complement the respiratory-deficient phenotype with mitochondrial iron accumulation and iron-sulfur protein defects that are otherwise associated with the lack of endogenous yeast frataxin (44). We can, therefore, conclude that assembly and iron-binding are relevant to human frataxin's ability to restore mitochondrial iron homeostasis in the yeast model of FRDA. In addition, the presence of a high-MW pool of frataxin in mouse heart suggests that frataxin assembly can occur not only during expression in *E.coli* or *S.cerevisiae* but also when frataxin is expressed at physiologic levels under native conditions. It is therefore reasonable to conclude that assembly and iron-binding are specific properties of frataxin.

A large body of experimental evidence from the yeast model of FRDA indicates that frataxin is critically involved in multiple aspects of iron and energy metabolism, namely, the conservation of cytoplasmic iron levels via stimulation of mitochondrial iron efflux (3,11,47), maintenance of iron-sulfur cluster-containing enzymes and oxidative phosphorylation (13,14,48), and protection from iron-induced oxidative damage (3). Similar observations have been made in the human disease. Elevated serum transferrin receptor levels, indicative of a limited cytoplasmic iron supply (20,21), and increased protoporphyrin levels, indicative of impaired heme synthesis (49), have been noted in FRDA patients. Signs of increased oxidative damage, including loss of mitochondrial DNA and iron-sulfur cluster-containing enzyme defects, have been observed in FRDA heart (19,26,27), while hypersensitivity to oxidative stress has been demonstrated in cultured FRDA cells (23). The pathogenic role of oxidative damage in FRDA is underscored by a study in which the antioxidant idebenone led to a decrease in myocardial hypertrophy in three patients (50), and a second study in which increased concentrations of 8-hydroxy-2′-deoxyguanosine, a marker of oxidative DNA damage, were noted in urine of 33 patients and were found decreased after idebenone administration (24). Granular iron deposits suggestive of mitochondrial iron overload can be detected in heart and other tissues from FRDA patients (18,19), and evidence of impaired mitochondrial iron homeostasis has also been found in cultured FRDA cells (22,23,51). Similarly, neuron/cardiac frataxin deficient mice develop early iron-sulfur cluster-containing enzyme defects and time-dependent mitochondrial iron accumulation (10).

Our findings provide a lead to explain the apparent involvement of frataxin in such diverse processes as cellular iron homeostasis, iron-sulfur cluster maintenance, energy metabolism and protection from oxidative damage. By functioning as an iron storage protein, frataxin could be able to keep iron in bioavailable and non-toxic form, just like ferritin. Moreover, by performing this function in the mitochondrial matrix, frataxin could play overlapping roles in heme and/or iron-sulfur cluster biogenesis and thus energy metabolism. Conversely, a deficiency of frataxin might favor iron participation in oxygen radical reactions and over time lead to accumulation of insoluble iron oxides within mitochondria. It has been suggested that continuous

oxidative damage to iron-sulfur clusters from impaired induction of superoxide dismutase genes may contribute to mitochondrial iron accumulation in frataxin-deficient cells (16). Our findings further suggest that lack of frataxin may cause mitochondrially-generated $O_2^{\cdot -}$ to preferentially react with excess Fe^{3+} in the mitochondrial matrix. This reaction could interfere with signaling to the SOD genes and at the same time promote Fenton chemistry by recycling Fe^{3+} to Fe^{2+} (52).

The existence of mitochondrial iron ligands required to maintain iron in bioavailable and non-toxic form has been postulated since early studies showing that approximately one-third of the total mitochondrial iron is not bound in heme or iron-sulfur clusters and is bioavailable (46,53). A recently identified human mitochondrial ferritin could play an important role in mitochondrial iron management (54). The fact that this protein has a limited tissue distribution (54), however, implies the existence of additional iron ligands. Flatmark and Romslo (53) reported previously that a hydrophilic molecule with MW $>10^6$, different from ferritin, might represent the main iron ligand in the matrix of rat liver mitochondria. Frataxin has a broad tissue distribution and is particularly induced in tissues with high oxygen consumption (2) and, therefore, represents an ideal candidate to perform this role (5). The assembly and iron-binding properties of human frataxin are consistent with this model and should provide a framework for future studies to address the mechanism of action of frataxin and the biochemical consequences of frataxin deficiency.

MATERIALS AND METHODS

Expression and purification of m-fxn

A DNA fragment including an ATG codon in frame with codons 56–210 of human frataxin was synthesized by PCR using a forward primer with an *Nde*I site (5′-ttattattacatatgagt-tcgaaccaacgtggcctc-3′) and a reverse primer with a stop codon and an *Eco*RI site (5′-ccgaattcattaagcatcttttccggaataggc-caagga-3′). This product was cloned downstream of the T7 promoter in vector pET24a(+) (Novagen) and sequenced completely. The resultant pETHF-2 vector was transformed into *E.coli* strain BL21(DE3) (Novagen) to produce the BL21(DE3)[pETHF-2] strain. Protein expression and purification were performed in three chromatographic steps including Macro-Prep DEAE (Bio-Rad), High Q (Bio-Rad), and Superdex 200 (Amersham Pharmacia Biotech), as described for yeast frataxin (28) with the modifications noted below. The bacterial lysate was loaded onto a Macro-Prep DEAE column, and a 1 l linear gradient, from 50 to 550 mM NaCl, in 20 mM Tris–HCl pH 8.0, 5 mM mannitol, was applied. The protein was eluted at a flow rate of 10 ml/min in two main pools, from 91 to 166 mM NaCl (low-salt DEAE pool; 170 ml), and from 380 to 500 mM NaCl (high-salt DEAE pool; 180 ml). Each pool was diluted to 600 ml and separately loaded onto a High Q column, and a 500 ml linear NaCl gradient was applied as described above. Most m-fxn from the low-salt DEAE pool eluted between 111 and 178 mM NaCl (low-salt High Q pool), and most m-fxn from the high-salt DEAE pool between 432 and 550 mM NaCl (high-salt High Q pool). These two pools were concentrated to 1 ml each by ultrafiltration, they were separately loaded onto a Superdex 200 column and eluted with 10 mM HEPES–KOH pH 7.4, 150 mM NaCl, 5 mM mannitol, at a flow rate of 1.5 ml/min. Low- and high-MW pools were recovered from the low- and high-salt High Q pools, respectively. The purified protein was stored at a concentration of ~0.5–2 mg/ml at room temperature (high-MW m-fxn) or 4°C (low-MW m-fxn). This procedure was reproducible regarding yield (~1 mg for high-MW and ~2.5 mg for low-MW m-fxn) and purity (>90%). Protein concentration was determined by the BCA kit (Pierce). ESI-MS and ICP were performed on m-fxn samples as previously described (28). For Sephacryl 300 chromatography, we used a 16 mm × 60 cm Sephacryl S-300 HR column from Amersham Pharmacia Biotech. The high-salt High Q pool was concentrated to 1 ml and loaded on this column, and protein was eluted with 10 mM HEPES–KOH pH 7.4, 150 mM NaCl, 5 mM mannitol, at a flow rate of 0.5 ml/min.

In vitro iron loading, native PAGE and western blotting

High-MW m-fxn (10–100 μM) was aerobically incubated with ferrous ammonium sulfate (Fe:m-fxn ratio of 10:1) in 10 mM HEPES–KOH pH 7.4, for 2 h at room temperature or 1 h at 30 or 37°C. Samples were centrifuged at 20 800 *g* for 10 min at 4°C to eliminate insoluble material, and aliquots of the supernatant were analyzed for iron and protein content by ICP and SDS–PAGE, respectively. In some experiments, iron-loaded m-fxn was re-isolated by gel filtration and its iron and protein content determined by ICP and SDS–PAGE. Similar iron:protein ratios were obtained by these procedures. Iron loading of horse spleen apoferritin (Sigma) was carried out as described (33). For native PAGE we used a discontinuous system consisting of a 3.8% T stacking gel (pH 6.8) and a 7% or 5% T separating gel (pH 8.9) prepared from a 40:1.7 ratio acrylamide:bisacrylamide stock solution. Electrophoresis was started at 100 V, shifted to 200 V after the samples had entered the separating gel, and continued for an additional 120 (7% PAGE) or 180 min (5% PAGE) after the dye had reached the bottom of the gel (12.5 cm total length). Gels were soaked for 30 min in 192 mM glycine, 25 mM Tris Base, 0.1% SDS prior to protein staining with Sypro Orange (Molecular Probes). For iron staining, gels were incubated with a freshly prepared solution of 100 mM potassium ferricyanide in 0.1 M HCl for 60 min in the dark at room temperature, rinsed with water, and dried (54). Dried gels were scanned in a ScanJet ADF (Hewlett Packard). For western blotting, native gels were soaked for 30 min in 120 mM glycine, 15.6 mM Tris Base, 0.1% SDS, 20% methanol, and blotted onto a polyvinylidene fluoride membrane (Millipore) in the same buffer.

Electron microscopy

Carbon-coated grids were glow-discharge activated (55). Samples (5 μl; ~0.1 mg/ml) were applied and allowed to absorb for 30 s, after which samples were stained with 2% uranyl acetate and examined in a Philips CM100 electron microscope at 80 kV. Unstained samples were examined directly after absorption. Images were recorded using a MegaView II CCD camera at a primary magnification of 64 000× corresponding to a pixel size of 0.97 nm.

In vivo analyses

For *in vivo* analysis of human frataxin, strain *yfh1*Δ[FRDA] (44) was grown in 10 ml of 1% yeast extract, 2% peptone, 2% dextrose, at 30°C to an OD_{600} of 3–5. Cells were harvested by centrifugation, washed with water and diluted to ~1 g (wet weight) per ml in 10 mM HEPES–KOH pH 7.4, 5 mM mannitol, containing one tablet per 50 ml of complete EDTA-free protease inhibitors (Boehringer Mannheim). Glass beads (350 mg of 425–600 µm beads; Sigma) were added to 500 µl of this suspension in an Eppendorf tube and the cells were broken by vortexing four times for 1 min at room temperature with 1 min intervals on ice. Beads and cell debris were removed by centrifugation for 5 min at 420 *g*, and 1% Triton X-100 was added to the samples that were subsequently incubated for 30 min on ice and finally centrifuged for 30 min at 100 000 *g* at 4°C. The supernatant (~12 mg total protein) was collected, further clarified through a 0.22 µm filter (Costar), and immediately analyzed on a 7.5 mm × 30 cm column packed with 13 ml of Superdex 200. 500 µl total extract were loaded on the column and proteins were eluted with 14 ml of 10 mM HEPES–KOH pH 7.4, 150 mM NaCl, 5 mM mannitol, containing one tablet per 50 ml of complete EDTA-free protease inhibitors, at a flow rate of 0.4 ml/min. Fractions (500 µl) were collected, concentrated to 50 µl by use of Ultrafree-0.5 cells (nominal MW limit 5000) (Millipore), and stored at –70°C. Fractions that eluted from the Superdex 200 column between the void volume and molecular mass ≥5 kDa were analyzed by 12.5% SDS–PAGE and western blotting as previously described (4). For immunoprecipitation of iron-loaded frataxin, the *yfh1*Δ[FRDA] strain was grown in medium supplemented with 31 µM $^{55}FeCl_3$ (NEN) and total cell extracts were prepared as described above, except that after treatment with Triton X-100 the homogenate was clarified by centrifugation for 10 min at 20 800 *g*. The supernatant (~13.5×10^6 c.p.m.) was pre-treated with 100 µl of protein A–Sepharose beads for 1 h at room temperature. After removal of the beads, the supernatant was incubated with 10 µl of anti-human frataxin antiserum for 10 h at 4°C, and immunocomplexes were precipitated by an additional 100 µl of protein A–Sepharose. After removal of the beads, the supernatant, which still contained >90% of the c.p.m. present before treatment with protein A–Sepharose, was further treated with 10 µl of a rabbit pre-immune serum for 10 h at 4°C, followed by 100 µl of protein A–Sepharose. At each step, protein A–Sepharose beads were washed twice with 10 mM HEPES–KOH pH 7.4, 100 mM NaCl, resuspended in buffer, and counted. For calculations, 1 µl of the $^{55}FeCl_3$ stock was also counted (~9×10^6 c.p.m. = 6 nmol Fe). The total mitochondrial iron present in each extract was estimated as follows. We showed previously that the *yfh1*Δ[FRDA] strain contains 1.3 nmol Fe/mg mitochondrial protein (44), and we know that under the growth conditions used for ^{55}Fe labeling this strain typically yields ~0.07 mg mitochondrial protein/ml of culture. Each of the extracts subjected to immunoprecipitation was prepared from a 10 ml culture, corresponding to ~0.7 mg mitochondrial protein and, thus, ~0.9 nmol mitochondrial iron.

Hearts were derived from wild-type C57BL6 mice in compliance with institutional guidelines and stored at –70°C. Frozen tissue was minced with a razor blade and homogenized in 500 µl of ice-cold 10 mM HEPES–KOH pH 7.4, 5 mM mannitol, containing one tablet per 50 ml of complete EDTA-free protease inhibitors. Following centrifugation at 420 *g* for 5 min, 1% Triton X-100 was added to the supernatant which was subsequently incubated for 30 min on ice, and centrifuged at 100 000 *g* for 30 min at 4°C. Protein concentration was determined in the supernatant and 10 mg total protein (final volume 500 µl) was analyzed by gel filtration and western blotting as described above for total yeast extracts.

To produce polyclonal antibodies against human frataxin, isolated m-fxn was injected into two rabbits. Total immune sera from these animals recognized a protein of ~17 kDa, that we have shown previously to correspond to the form of frataxin detected in human tissues (4). Monoclonal anti-yeast Pgk1p antibody was purchased from Molecular Probes. Polyclonal antibodies against SCAD were a generous gift of Dr G.Vockley, Mayo Clinic, Rochester, MN.

ACKNOWLEDGEMENTS

We thank J.Adamec and O.Gakh for help and discussions, J.Drysdale for suggestions on the Prussian Blue staining procedure, and G.Vockley for anti-SCAD antibodies. This work was supported by Institutional Research Concept no. AV0Z5020903 (to O.B.), a fellowship from the Pierfranco e Luisa Mariani Foundation, Milan, Italy (to P.C.), and grants from the MDA and the NIH/NIA (AG15709) (to G.I.).

REFERENCES

1. Harding,A.E. (1981) Friedreich's ataxia: a clinical and genetic study of 90 families with an analysis of early diagnostic criteria and intrafamilial clustering of clinical features. *Brain*, **104**, 589–620.
2. Campuzano,V., Montermini,L., Molto,M.D., Pianese,L., Cossee,M., Cavalcanti,F., Monros,E., Rodius,F., Duclos,F., Monticelli,A. *et al.* (1996) Friedreich's ataxia: autosomal recessive disease caused by an intronic GAA triplet repeat expansion. *Science*, **271**, 1423–1427.
3. Babcock,M., de Silva,D., Oaks,R., Davis-Kaplan,S., Jiralerspong,S., Montermini,L., Pandolfo,M. and Kaplan,J. (1997) Regulation of mitochondrial iron accumulation by Yfh1p, a putative homolog of frataxin. *Science*, **276**, 1709–1712.
4. Cavadini,P., Adamec,J., Taroni,F., Gakh,O. and Isaya,G. (2000) Two-step processing of human frataxin by mitochondrial processing peptidase: precursor and intermediate forms are cleaved at different rates. *J. Biol. Chem.*, **275**, 41469–41475.
5. Patel,P.I. and Isaya,G. (2001) Friedreich ataxia: from GAA triplet-repeat expansion to frataxin deficiency. *Am. J. Hum. Genet.*, **69**, 1.
6. Gibson,T.J., Koonin,E.V., Musco,G., Pastore,A. and Bork,P. (1996) Friedreich's ataxia protein: phylogenetic evidence for mitochondrial dysfunction. *Trends Neurosci.*, **19**, 465–468.
7. Foury,F. and Cazzalini,O. (1997) Deletion of the yeast homologue of the human gene associated with Friedreich's ataxia elicits iron accumulation in mitochondria. *FEBS Lett.*, **411**, 373–377.
8. Koutnikova,H., Campuzano,V., Foury,F., Dolle,P., Cazzalini,O. and Koenig,M. (1997) Studies of human, mouse and yeast homologues indicate a mitochondrial function for frataxin. *Nat. Genet.*, **16**, 345–351.
9. Wilson,R.B. and Roof,D.M. (1997) Respiratory deficiency due to loss of mitochondrial DNA in yeast lacking the frataxin homologue. *Nat. Genet.*, **16**, 352–357.
10. Puccio,H., Simon,D., Cossee,M., Criqui-Filipe,P., Tiziano,F., Melki,J., Hindelang,C., Matyas,R., Rustin,P. and Koenig,M. (2001) Mouse models of Friedreich ataxia exhibit cardiomyopathy, sensory nerve defect and Fe-S enzyme deficiency followed by intramitochondrial iron deposits. *Nat. Genet.*, **27**, 181–186.
11. Radisky,D.C., Babcock,M.C. and Kaplan,J. (1999) The yeast frataxin homologue mediates mitochondrial iron efflux. Evidence for a mitochondrial iron cycle. *J. Biol. Chem.*, **274**, 4497–4499.
12. Chen,O.S. and Kaplan,J. (2000) CCC1 suppresses mitochondrial damage in the yeast model of Friedreich's ataxia by limiting mitochondrial iron accumulation. *J. Biol. Chem.*, **275**, 7626–7632.

13. Foury,F. (1999) Low iron concentration and aconitase deficiency in a yeast frataxin homologue deficient strain. *FEBS Lett.*, **456**, 281–284.
14. Lutz,T., Westermann,B., Neupert,W. and Herrmann,J.M. (2001) The mitochondrial proteins Ssq1 and Jac1 are required for the assembly of iron sulfur clusters in mitochondria. *J. Mol. Biol.*, **307**, 815–825.
15. Huynen,M.A., Snel,B., Bork,P. and Gibson,T.J. (2001) The phylogenetic distribution of frataxin indicates a role in iron-sulfur cluster protein assembly. *Hum. Mol. Genet.*, **10**, 2463–2468.
16. Chantrel-Groussard,K., Geromel,V., Puccio,H., Koenig,M., Munnich,A., Rotig,A. and Rustin,P. (2001) Disabled early recruitment of antioxidant defenses in Friedreich's ataxia. *Hum. Mol. Genet.*, **10**, 2061–2067.
17. Ristow,M., Pfister,M.F., Yee,A.J., Schubert,M., Michael,L., Zhang,C.Y., Ueki,K., Michael,M.D.,II, Lowell,B.B. and Kahn,C.R. (2000) Frataxin activates mitochondrial energy conversion and oxidative phosphorylation. *Proc. Natl Acad. Sci. USA*, **97**, 12239–12243.
18. Lamarche,J.B., Cote,M. and Lemieux,B. (1980) The cardiomyopathy of Friedreich's ataxia morphological observations in 3 cases. *Can. J. Neurol. Sci.*, **7**, 389–396.
19. Bradley,J.L., Blake,J.C., Chamberlain,S., Thomas,P.K., Cooper,J.M. and Schapira,A.H. (2000) Clinical, biochemical and molecular genetic correlations in Friedreich's ataxia. *Hum. Mol. Genet.*, **9**, 275–282.
20. Wilson,R.B., Lynch,D.R., Farmer,J.M., Brooks,D.G. and Fischbeck,K.H. (2000) Increased serum transferrin receptor concentrations in Friedreich ataxia. *Ann. Neurol.*, **47**, 659–661.
21. Scarano,V., de Cristofaro,T., De Michele,G., Salvatore,E., De Biase,I., Monticelli,A., Filla,A. and Cocozza,S. (2001) Serum transferrin receptor levels in Friedreich's and other degenerative ataxias. *Neurology*, **57**, 159–160.
22. Tan,G., Chen,L.S., Lonnerdal,B., Gellera,C., Taroni,F.A. and Cortopassi,G.A. (2001) Frataxin expression rescues mitochondrial dysfunctions in FRDA cells. *Hum. Mol. Genet.*, **10**, 2099–2107.
23. Wong,A., Yang,J., Cavadini,P., Gellera,C., Lonnerdal,B., Taroni,F. and Cortopassi,G. (1999) The Friedreich's ataxia mutation confers cellular sensitivity to oxidant stress which is rescued by chelators of iron and calcium and inhibitors of apoptosis. *Hum. Mol. Genet.*, **8**, 425–430.
24. Schultz,J.B., Dehmer,T., Schols,L., Mende,H., Hardt,C., Vorgerd,M., Burk,K., Matson,W., Dichgans,J., Beal,M.F. and Bogdanov,M.B. (2000) Oxidative stress in patients with Friedreich's ataxia. *Neurology*, **55**, 1719–1721.
25. Emond,M., Lepage,G., Vanasse,M. and Pandolfo,M. (2000) Increased levels of plasma malondialdehyde in Friedreich ataxia. *Neurology*, **55**, 1752–1753.
26. Rotig,A., de Lonlay,P., Chretien,D., Foury,F., Koenig,M., Sidi,D., Munnich,A. and Rustin,P. (1997) Aconitase and mitochondrial iron-sulfur protein deficiency in Friedreich ataxia. *Nat. Genet.*, **17**, 215–217.
27. Lodi,R., Cooper,J.M., Bradley,J.L., Manners,D., Styles,P., Taylor,D.J. and Schapira,A.H. (1999) Deficit of in vivo mitochondrial ATP production in patients with Friedreich ataxia. *Proc. Natl Acad. Sci. USA*, **96**, 11492–11495.
28. Adamec,J., Rusnak,F., Owen,W.G., Naylor,S., Benson,L.M., Gacy,A.M. and Isaya,G. (2000) Iron-dependent self-assembly of recombinant yeast frataxin: implications for Friedreich ataxia. *Am. J. Hum. Genet.*, **67**, 549–562.
29. Sherman,F., Stewart,J.W. and Tsunasawa,S. (1985) Methionine or not methionine at the beginning of a protein. *Bioessays*, **3**, 27–31.
30. Musco,G., Stier,G., Kolmerer,B., Adinolfi,S., Martin,S., Frenkiel,T., Gibson,T. and Pastore,A. (2000) Towards a structural understanding of Friedreich's ataxia: the solution structure of frataxin. *Struct. Fold. Des.*, **8**, 695–707.
31. Edmonds,C.G. and Smith,R.D. (1990) Electrospray ionization mass spectrometry. *Methods Enzymol.*, **193**, 412–431.
32. Hudson,A.J., Andrews,S.C., Hawkins,C., Williams,J.M., Izuhara,M., Meldrum,F.C., Mann,S., Harrison,P.M. and Guest,J.R. (1993) Overproduction, purification and characterization of the *Escherichia coli* ferritin. *Eur. J. Biochem.*, **218**, 985–995.
33. Levi,S., Salfeld,J., Franceschinelli,F., Cozzi,A., Dorner,M.H. and Arosio,P. (1989) Expression and structural and functional properties of human ferritin L-chain from *Escherichia coli*. *Biochemistry*, **28**, 5179–5184.
34. Rucker,P., Torti,F.M. and Torti,S.V. (1997) Recombinant ferritin: modulation of subunit stoichiometry in bacterial expression systems. *Protein Eng.*, **10**, 967–973.
35. Andrews,S.C. (1998) Iron storage in bacteria. *Adv. Microb. Physiol.*, **40**, 281–351.
36. Petrat,F., de Groot,H. and Rauen,U. (2001) Subcellular distribution of chelatable iron: a laser scanning microscopic study in isolated hepatocytes and liver endothelial cells. *Biochem. J.*, **356**, 61–69.
37. Harrison,P.M. and Arosio,P. (1996) The ferritins: molecular properties, iron storage function and cellular regulation. *Biochim. Biophys. Acta*, **1275**, 161–203.
38. Dhe-Paganon,S., Shigeta,R., Chi,Y.I., Ristow,M. and Shoelson,S.E. (2000) Crystal structure of human frataxin. *J. Biol. Chem.*, **275**, 30753–30756.
39. Williams,M.A. and Harrison,P.M. (1968) Electron-microscopic and chemical studies of oligomers in horse ferritin. *Biochem. J.*, **110**, 265–280.
40. Thomas,B.R., Carter,D. and Rosenberger,F. (1998) Effect of microheterogeneity on horse spleen apoferritin crystallization. *J. Crystal Growth*, **187**, 499–510.
41. Petsev,D.N., Thomas,B.R., Yau,S. and Vekilov,P.G. (2000) Interactions and aggregation of apoferritin molecules in solution: effects of added electrolytes. *Biophys. J.*, **78**, 2060–2069.
42. Baneyx,F., Bertsch,U., Kalbach,C.E., van der Vies,S.M., Soll,J. and Gatenby,A.A. (1995) Spinach chloroplast cpn21 co-chaperonin possesses two functional domains fused together in a toroidal structure and exhibits nucleotide-dependent binding to plastid chaperonin 60. *J. Biol. Chem.*, **270**, 10695–10702.
43. Kim,Y.W., Kang,K.S., Kim,S.Y. and Kim,I.S. (2000) Formation of fibrillar multimers of oat beta-glucosidase isoenzymes is mediated by the As-Glu1 monomer. *J. Mol. Biol.*, **303**, 831–842.
44. Cavadini,P., Gellera,C., Patel,P.I. and Isaya,G. (2000) Human frataxin maintains mitochondrial iron homeostasis in *Saccharomyces cerevisiae*. *Hum. Mol. Genet.*, **9**, 2523–2530.
45. Battaile,K.P., Mohsen,A.W. and Vockley,J. (1996) Functional role of the active site glutamate-368 in rat short chain acyl-CoA dehydrogenase. *Biochemistry*, **35**, 15356–15363.
46. Tangeras,A. (1985) Mitochondrial iron not bound in heme and iron-sulfur centers and its availability for heme synthesis *in vitro*. *Biochim. Biophys. Acta*, **843**, 199–207.
47. Foury,F. and Talibi,D. (2001) Mitochondrial control of iron homeostasis. A genome wide analysis of gene expression in a yeast frataxin-deficient strain. *J. Biol. Chem.*, **276**, 7762–7768.
48. Branda,S.S., Yang,Z.Y., Chew,A. and Isaya,G. (1999) Mitochondrial intermediate peptidase and the yeast frataxin homolog together maintain mitochondrial iron homeostasis in *Saccharomyces cerevisiae*. *Hum. Mol. Genet.*, **8**, 1099–1110.
49. Morgan,R.O., Naglie,G., Horrobin,D.F. and Barbeau,A. (1979) Erythrocyte protoporphyrin levels in patients with Friedreich's and other ataxias. *J. Can. Sci. Neurol.*, **6**, 227–232.
50. Rustin,P., von Kleist-Retzow,J.C., Chantrel-Groussard,K., Sidi,D., Munnich,A. and Rotig,A. (1999) Effect of idebenone on cardiomyopathy in Friedreich's ataxia: a preliminary study. *Lancet*, **354**, 477–479.
51. Delatycki,M.B., Camakaris,J., Brooks,H., Evans-Whipp,T., Thorburn,D.R., Williamson,R. and Forrest,S.M. (1999) Direct evidence that mitochondrial iron accumulation occurs in Friedreich ataxia. *Ann. Neurol.*, **45**, 673–675.
52. Halliwell,B. and Gutteridge,J.M.C. (1999) Chemistry of biologically important radicals. In *Free Radicals in Biology and Medicine.* Oxford University Press, Oxford, UK, pp. 48–82.
53. Flatmark,T. and Romslo,I. (1975) Energy-dependent accumulation of iron by isolated rat liver mitochondria. Requirement of reducing equivalents and evidence for a unidirectional flux of Fe(II) across the inner membrane. *J. Biol. Chem.*, **250**, 6433–6438.
54. Levi,S., Corsi,B., Bosisio,M., Invernizzi,R., Volz,A., Sanford,D., Arosio,P. and Drysdale,J. (2001) A human mitochondrial ferritin encoded by an intronless gene. *J. Biol. Chem.*, **25**, 24437–24440.
55. Benada,O. and Pokorny,V. (1990) Modification of the Polaron Ssputter-coater unit for glow-discharge activation of carbon support films. *J. Electron Microsc. Tech.*, **16**, 235–239.